



Enhanced recombinant expression and purification of human IRAP for biochemical and crystallography studies

Lufei Sui¹, Hwai-Chen Guo^{*}

Department of Biological Sciences, University of Massachusetts Lowell, 1 University Avenue, Lowell, MA, 01854, USA

ARTICLE INFO

Keywords:

Insulin-regulated aminopeptidase (IRAP)
Expression and purification
Substrate affinity
Crystallization
Peptide inhibitor
Cognitive enhancers

ABSTRACT

Insulin-regulated aminopeptidase (IRAP) in humans is a membrane bound enzyme that has multiple functions. It was first described as a companion protein of the insulin-responsive glucose transporter, Glut4, in specialized vesicles. The protein has subsequently been shown to be identical to the oxytocinase/aminopeptidase or the angiotensin IV (Ang IV) receptor (AT₄ receptor). Some AT₄ ligand peptides, such as Ang IV and LVV-hemorphin-7, have been shown to act as IRAP inhibitors that exert memory-enhancing properties. As such IRAP has been a target for developing cognitive enhancers. To facilitate detailed mechanistic studies of IRAP catalysis and inhibition, and to pave the way for biophysical and structural studies of IRAP in complex with peptide inhibitors, we report here an optimized expression and purification system using High Five insect cells. We also report biochemical characterizations of the purified recombinant IRAP with a standard aminopeptidase substrate and an optimized IRAP peptide inhibitor with a Ki of 98 nM.

1. Introduction

Insulin-regulated aminopeptidase (IRAP, EC 3.4.11.3) in humans is a transmembrane protein with broad tissue distribution and has a dual function [1]. Its N-terminal domain is a 109-amino acid cytoplasmic domain, followed by a short transmembrane domain of 23 amino acids, along with a large 893-amino acid extracellular or intraluminal domain, depending on its localization in the cell (Fig. 1A). As a result, IRAP mainly exists as a membrane-attached enzyme either in endosomes or on the cell surface. Nonetheless, in placental serum, a soluble form of IRAP has also been detected, with 154F/155A identified as the cleavage site by the ADAM family of endopeptidase [2]. The N-terminal cytoplasmic domain of IRAP plays a role in intracellular trafficking, whereas its C-terminal extracellular/intraluminal domain is responsible for the aminopeptidase activity to trim peptides. IRAP together with ERAP1 (ER aminopeptidase 1) and ERAP2 (ER aminopeptidase 2) are classified into the distinct oxytocinase subfamily of M1 Zinc aminopeptidases [3,4]. With the exception of the N-terminal cytoplasmic and the transmembrane domains in IRAP, these three aminopeptidases are highly

homologous. They share nearly 50% of overall sequence identity, with a conserved Zn²⁺ binding motif and the GAMEN exopeptidase motif located at the catalytic site of the protein extracellular/intraluminal domain. Moreover, the genes coded for these three aminopeptidases are located contiguously on human chromosome 5q15 [3].

All three members of oxytocinase subfamily have been implicated in immune responses [4]. Residing inside the ER, ERAP1 and ERAP2 are regulated by IFN- γ responses and are involved in the final processing of peptidomes to be presented by MHC class I (MHC-I) molecules via the endogenous presentation pathway [5]. In contrast, IRAP does not respond to IFN- γ stimulation. Studies have shown that IRAP is not involved in the MHC-I endogenous presentation pathway [6]. Instead, IRAP has been shown to be involved in the MHC-I cross-presentation pathway, consistent with its intracellular localization in phagosomes and endosomes [6,7].

IRAP also plays important roles outside of immunity. It degrades hormone peptides such as oxytocin (OT) in placental serum in order to maintain a homeostasis condition during pregnancy. Currently, IRAP is the only known M1 aminopeptidase that can cleave OT and other cyclic

Abbreviations: Ang IV, angiotensin IV; AT₄, Ang IV receptor; ERAP, endoplasmic reticulum aminopeptidase; IEX, ion exchange chromatography; IMAC, immobilized metal ion affinity chromatography; IRAP, insulin-regulated aminopeptidase; L-AMC, leucine 7-amido-4-methylcoumarin; LVV-H7, LVV-hemorphin-7; MHC-I, major histocompatibility complex class I; SEC, size exclusion chromatography.

* Corresponding author. Department of Biological Sciences, University of Massachusetts Lowell, Lowell, MA, 01854, USA.

E-mail address: HwaiChen_Guo@uml.edu (H.-C. Guo).

¹ Present Address: The Vascular Biology Program and Department of Surgery, Harvard Medical School, Boston Children's Hospital, 300 Longwood Avenue, Boston, MA, 02115, USA.

<https://doi.org/10.1016/j.bbrep.2021.101042>

Received 16 March 2021; Received in revised form 1 June 2021; Accepted 2 June 2021

2405-5808/© 2021 The Authors. Published by Elsevier B.V. This is an open access article under the CC BY-NC-ND license

(<http://creativecommons.org/licenses/by-nc-nd/4.0/>).

peptides with a cystine disulfide structure such as vasopressin [8]. Comparative studies indicates that conformation of the GAMEN motif in IRAP is more extended than that of either ERAP1 or ERAP2, resulting in a larger substrate pocket to fit cyclic peptides such as OT or vasopressin [9]. IRAP is also identified as the angiotensin IV (Ang IV) receptor (AT₄ receptor) [10]. Through IRAP mediation, Ang IV is involved in a wide range of physiological activities, including facilitating memory. In addition, some IRAP ligands, including Ang IV (sequence: VYIHPF), Nle1-Ang IV, and the structurally distinct peptide LVV-hemorphin-7 (LVV-H7, sequence: LVVYPWTQRF), are not cleaved by IRAP and therefore are potential inhibitors of the IRAP activity with different binding affinity [11]. Based on the observations that its inhibitors exert memory-enhancing properties, IRAP has been a target for the development of cognitive enhancers [10,12]. Even though the mechanism of IRAP inhibition in memory enhancement is not completely understood, it was postulated to effect the preservation of neuropeptides from degradation consequently increasing their half-life. Therefore, screening IRAP inhibitors with memory-enhancing properties has been an active area of research [10,13,14]. Despite these biological and pharmacological significances, crystal structures of IRAP were only determined recently, and at a low-intermediate resolution (2.5–3.4 Å) [9,15,16]. Moreover, current systems to express and purify a soluble form of recombinant IRAP to support these biochemical and biophysical studies only lead to low yield using mammalian or insect cells. To facilitate studies on the mechanistic details of IRAP catalysis and inhibition, and to pave a way for high-resolution structural studies of IRAP in complex with various peptide inhibitors, we report here an efficient expression and purification system, and biochemical characterizations of the purified recombinant IRAP. We also co-crystallized IRAP with a short yet potent peptide that inhibits IRAP with a K_i of 98 nM.

2. Material and methods

2.1. Construction of baculovirus vector for expressing secreted IRAP in High Five insect cells

Bacmid DNA for IRAP expression in insect cells were generated using methods previously described [17,18] but with some modifications. To overcome low solubility issues, we generated baculovirus expression vector to secrete IRAP into the extracellular cell medium using a secretion signal sequence, honeybee melittin (HBM) [19]. For recombinant protein expression, we used the High Five cell line (BTI-TN-5B1-4) [20] grown in Express Five serum-free medium (Invitrogen, Waltham, MA) supplemented with 18 mM L-glutamine, and by infecting cells at a density of 2×10^6 cells/ml using P3 recombinant baculovirus at MOI 1. After 30hr post-infection, cell medium was collected for downstream protein purification.

2.2. Protein purification and optimization

High Five cell medium containing IRAP protein was first collected by centrifuging at 5000 g for 20min and then passed through a 0.22 µm filter to remove small cell particles. A special-purpose Ni Sepharose excel resin (GE Healthcare, Woburn, MA) was used to capture secreted IRAP that contains a C-terminal His₆-tag. The filtered cell medium was then slowly passed overnight through Ni Sepharose excel resin for thorough protein binding, followed by three washes using running buffer containing 50 mM Tris HCl pH 7.5, 500 mM NaCl and 10–30 mM imidazole. Afterward, the protein was eluted with running buffer containing 350 mM imidazole. Before IEX chromatography, protein samples from IMAC capture were dialyzed against 20 mM HEPES pH 7.2 for 4hr at 4 °C to reach a minimum ionic strength and followed by loading them onto an anion exchanger HiTrap Q HP column. Protein was then eluted using an ionic gradient with an increasing ionic strength up to 1 M NaCl for 10 CV at 1 ml/min. Afterward, IEX purified protein was concentrated using Amicon Ultra MWCO 30 KDa centrifugal filters to 12 mg/ml in 0.5 ml and applied to a Superdex S-200 size exclusion column (GE healthcare, Woburn, MA) with a flow rate 0.3 ml/min. Protein was eluted in buffer containing 10 mM Tris-HCl pH 7.2, 150 mM NaCl. Size and purity were confirmed by 8% Native PAGE and SDS PAGE. The peak fractions were pooled together and concentrated to 10 mg/ml using Amicon Ultra MWCO 50 KDa centrifugal filters. The protein concentration was determined by the BCA assay, as well as by absorbance measurement at 280 nm using NanoDrop 2000/2000c Spectrophotometer (Thermo Scientific, Waltham, MA) with an extinction coefficient of 1.67 mg/ml·OD₂₈₀.

2.3. Initial crystallization screens of IRAP-inhibitor complex

For complex crystallization, 15 µM IRAP was incubated with 80 µM peptide inhibitor VYPWT (synthesized by GeneScript) at room temperature for 1hr, followed by further concentrating to 10 mg/ml. The initial crystallization trials were performed at 23 °C in the solution containing 10 mM Tris, pH 8.5, and with different concentrations of PEG8000 or PEG3350, and with 1:1 protein/reservoir ratio.

2.4. Measurement of aminopeptidase activity by fluorescence assays

Binding constant K_m of purified IRAP was determined by the hydrolysis of fluorescent substrate leucine 7-amido-4-methylcoumarin (L-AMC) [21]. After cleavage by IRAP, the released fluorescent dye was detected with Emission 440 nm upon Excitation at 380 nm. Hydrolysis of substrate with a range of concentrations of L-AMC were performed in 96-well plate at 25 °C in 200 µl of 20 mM Tris, pH 8.0, 0.1 M NaCl, containing 62.5 ng of IRAP enzyme. Various concentrations of L-AMC

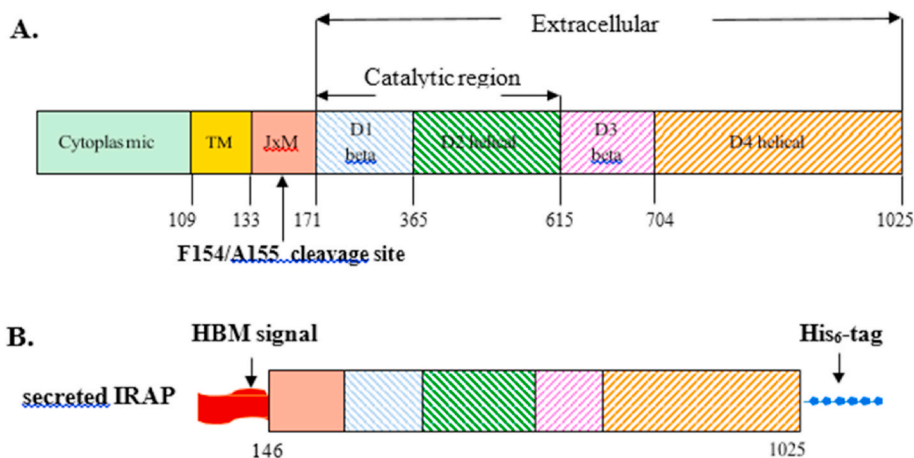


Fig. 1. Domain organization of IRAP and designed construct of the secreted recombinant IRAP. A. IRAP consists of a cytoplasmic domain, a transmembrane domain (TM), followed by a juxtamembrane region (JxM), and the large extracellular/intraluminal domain. The extracellular domain includes a catalytic site with a D1 β-sheet region and a D2 α-helical region, followed by a C-terminal domain with D3 β sheets and D4 α helices [26]. B. The engineered construct to express a soluble form of IRAP, with an HBM secretion signal sequence at the N-terminal end and a His₆ tag at the C-terminal end of the recombinant IRAP.

(5–500 μM) were added in the pre-incubated reactions followed by 30min incubation. Each condition was assayed in duplicates. The release of enzymatic product was detected by fluorescence microplate reader SpectraMax M2 (Molecular Devices, Sunnyvale, CA). V_{max} and K_{m} for L-AMC was determined by the Michaelis-Menten model using a Prism 8 software (<https://www.graphpad.com/scientific-software/prism/>).

2.5. Inhibition assays using peptide VYPWT

Inhibition of purified IRAP by the synthetic peptide VYPWT was determined using the fluorescent substrate L-AMC and various concentrations of the peptide inhibitor to calculate K_{i} . In a 200 μl reaction system, each well contained 62.5 ng of purified IRAP enzyme and 80 μM of substrate L-AMC. The extent of IRAP inhibition by peptide was determined over a range of peptide concentrations (0.1 nM–100 μM) in

triplicates. A control experiment with only substrate and enzyme but no peptide inhibitor was used as a reference for calculating % aminopeptidase activity. The IC_{50} value was calculated using the Prism 8 software. The inhibitor constant (K_{i}) was calculated by the relationship of $IC_{50} = K_{\text{i}} (1 + [S]/K_{\text{m}})$ [22], where K_{m} for L-AMC was determined from the experiments in the section above.

3. Results and discussion

3.1. Expression of recombinant IRAP

To express recombinant IRAP, we generated baculovirus vectors using the Bac-to-Bac expression system in insect cells. Although the closely related ERAP1 had been successfully expressed as a soluble protein in cytoplasm using this system [18,23], the same strategy

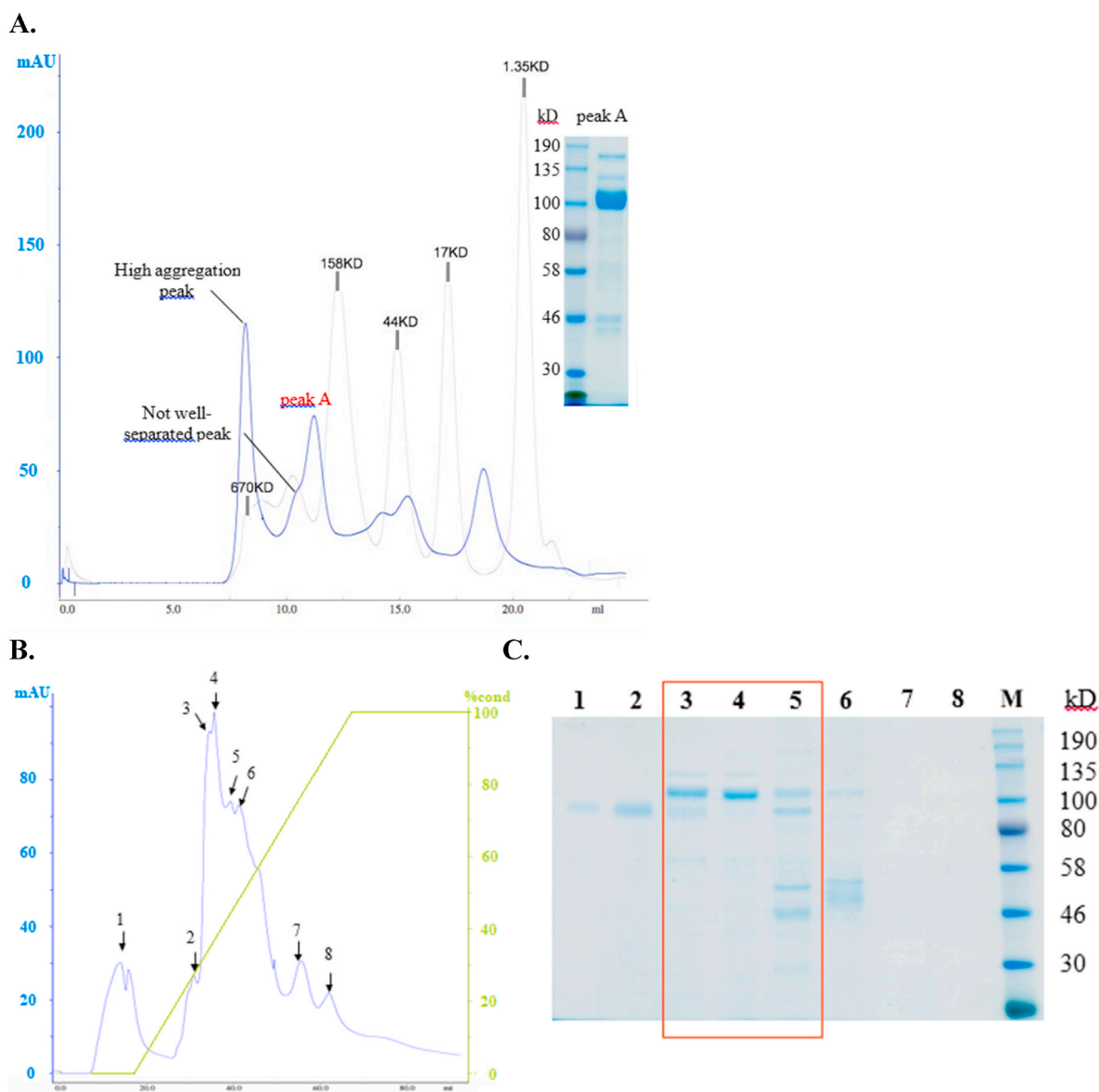


Fig. 2. Size exclusion and ion exchange chromatograms of secreted IRAP after the initial capture by IMAC. **A.** IMAC-captured IRAP was directly loaded onto a Superdex 200 SEC column and run at a rate of 0.3 ml/min. The protein eluate was monitored by UV absorbance at 280 nm. The light gray curve in the background marks the elution volumes of size standards, with their molecular sizes marked in kilodaltons (KD). Sample in peak A was analyzed by SDS-PAGE (the inset at top right). **B.** IMAC-captured IRAP was further purified using a HiTrap Q HP column with a linear gradient of NaCl from 0 to 1 M. The elution gradient is monitored by % conductivity (green slope & scales on the right-side of the plot, normalized to 100% @ 1 M NaCl). **C.** SDS-PAGE analysis of collected fractions from the IEX intermediate step. Fractions from (B) were analyzed by staining with Coomassie Blue stain. Note that IRAP was mainly eluted in fractions 3–5 (boxed in red). (For interpretation of the references to colour in this figure legend, the reader is referred to the Web version of this article.)

yielded insoluble recombinant IRAP (data not shown) even though these two proteins are highly homologous with a 43% sequence identity. Further sequence analyses suggested that this difference could be due to a relatively high glycosylation content in IRAP. Based on the NetNGlyc 1.0 Server for prediction of N-linked glycosylation sites [24], IRAP was predicted to contain 13 potential N-glycosylation sites whereas ERAP1 only has four potential N-linked glycosylation sites. Thus, it is plausible that the construct to express IRAP in cytoplasm mis-folded due to a deficiency in N-glycosylation [25]. To overcome this insolubility issue, we generated a new baculovirus vector to express IRAP as a secreted recombinant protein (Fig. 1B). We also used a different insect cell line, *Trichoplusia ni* BTI- TN-5B1-4 (High Five cells) since it was shown to produce 5–10 fold higher secreted expression levels of glycosylated proteins than Sf9 cells [20]. To this end, a strong insect secretory signal peptide from Honeybee Mellitin (HBM) was introduced at the N-terminal of IRAP to direct the protein through the ER and the Golgi complex for proper post-translational modifications and a final release into cell medium. A His₆ tag was also attached to the C-terminal end of IRAP for facilitating downstream protein purification (Fig. 1B).

3.2. Optimization of IRAP purification

Secreted IRAP in the media was first captured by IMAC (immobilized

metal ion chromatography) using a Ni Sepharose resin. We found the recombinant IRAP was co-purified with a major contaminant around 90kD, which appears to be a secreted protein from the host cells (data not shown). However, replacing the spent cell medium with fresh medium at 6hr post-infection was able to quickly remove bulk of this major contaminant protein.

When the IMAC purified protein was applied directly to a Superdex200 size exclusion column, there was a large aggregation peak as well as poor separation indicated by a peak with a shoulder (peak A in Fig. 2A). As shown by the SDS-PAGE analysis (inset in Fig. 2A), there were still some contaminant proteins after the direct gel filtration chromatography. Thus, we applied an anion exchange chromatography (IEX) as an intermediate purification step before the final polishing step of SEC (size exclusion chromatography). As shown in the IEX chromatogram with a linear elution gradient of increasing NaCl concentration (Fig. 2B), multiple elution peaks were detected. All the peaks, even though not fully separated, were collected and analyzed on SDS PAGE (Fig. 2C). The recombinant IRAP protein was detected mainly in peak fractions 3–5, corresponding to 0.3–0.5 M NaCl gradient (Fig. 2C). As a compromise between protein purity and yield, only fractions 3–5 were pooled together for further polishing with a SEC column. To reduce band broadening on the following SEC step, the IRAP eluent from IEX was concentrated up to 12 mg/ml, which had a high recovery without a loss

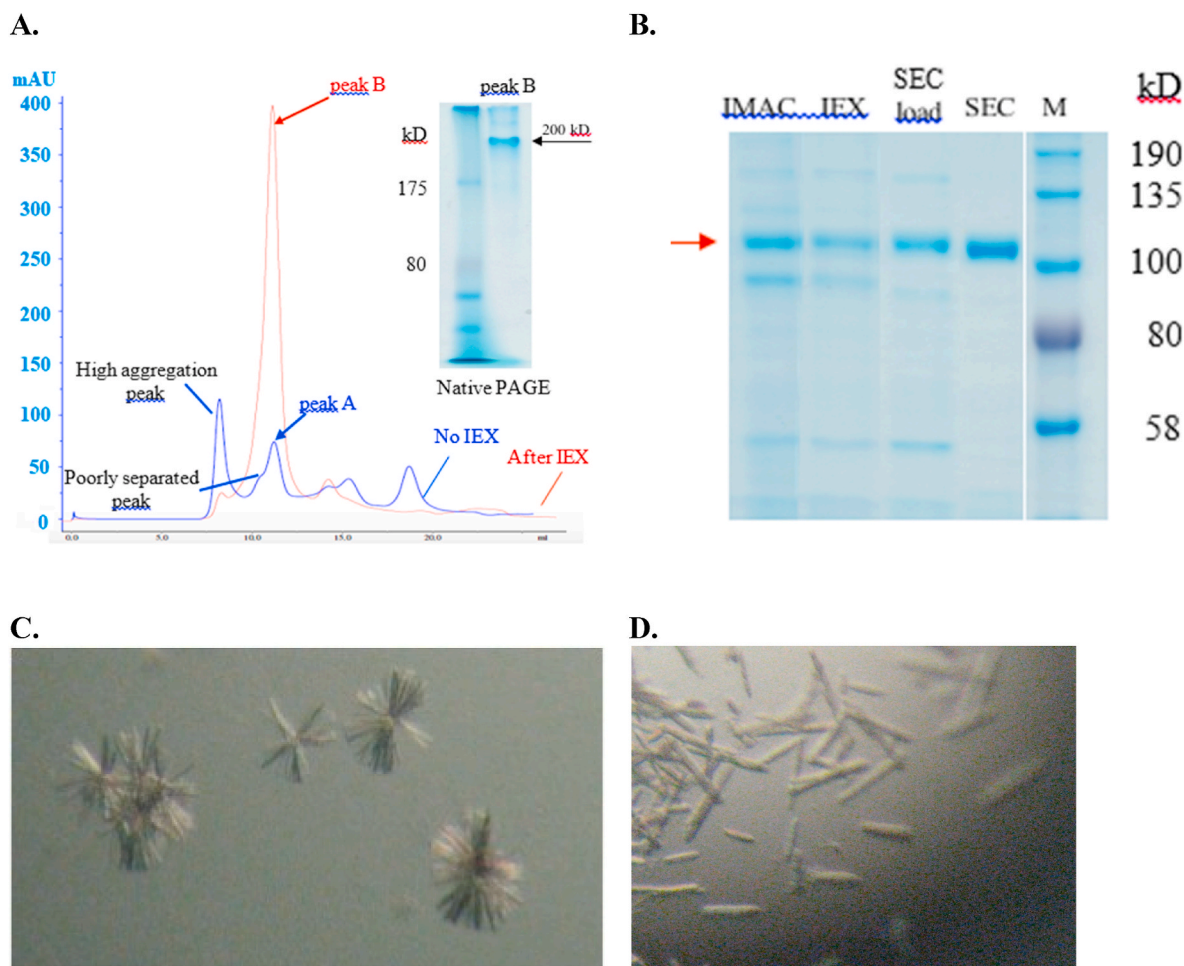


Fig. 3. Three-step purification of IRAP, and initial crystallization trials of IRAP-peptide complex. A. Comparison of final SEC purifications of IRAP with (red chromatogram) or without (blue chromatogram) an intermediate step of ion exchange chromatography (IEX). Sample in peak B was analyzed by native PAGE analysis (the inset at top right). B. Optimized purification of IRAP by three consecutive steps of chromatography. Samples eluted from the initial IMAC capture, the intermediate IEX purification, the concentrated IEX eluents before SEC loading, and the purified IRAP after the final polishing SEC step were analyzed by SDS-PAGE and stained with Coomassie Blue stain. Approximately same amounts of total protein were loaded in each lane. C. Needle-like crystals were obtained 5 days after the initial set-up of incubating IRAP with a peptide inhibitor (VYPWT). D. Small but single crystals were obtained after crystallization refinement in combination with micro-seeding techniques. (For interpretation of the references to colour in this figure legend, the reader is referred to the Web version of this article.)

of enzyme specific activity (data not shown).

Finally, the concentrated protein was subjected to a polishing step by SEC. As shown in the SEC chromatogram (Fig. 3A), with an additional intermediate step of IEX there was less aggregation and the peak containing IRAP (peak B) is larger and better resolved from other protein peaks. Interestingly, the protein was eluted around 11 ml, corresponding to a size of ~200 kDa that is about twice the size of calculated molecular weight and apparent size on SDS PAGE (Fig. 2A and C). Further analysis by native PAGE also appears to be an IRAP dimer (inset in Fig. 3A). This is consistent with recent findings of IRAP dimeric structure and its physiological form [9,15,26,27]. As shown in Fig. 3B, the purity of IRAP, analyzed by SDS PAGE, gradually increased with each purification step, with no obvious contaminant protein after the final SEC polishing. Improved purity (measured by specificity activity U/mg) following the IMAC, IEX, and SEC steps are measured to be 61x, 1.2x, and 2.3x, respectively. Overall the enzyme specific activities increased by about 170 fold, from 5.4 to 920.5 U/mg.

3.3. Crystallization of IRAP-peptide inhibitor

To test the quality of the purified recombinant IRAP, and to pave the way for future biophysical and structural studies of IRAP inhibition mechanism by peptide inhibitors, we initiated crystallization screen of IRAP-inhibitor complex, by mixing a short peptide inhibitor VYPWT (see below) with IRAP in the crystallization setup. In the initial trials, crystal-like needles (Fig. 3C) grew after 5 days in drops with the reservoir solution of 10 mM Tris, pH 8.5, 100 mM NaCl, 20% PEG8000 or 10 mM Tris, pH 8.5, 100 mM NaCl, 25% PEG3350. A further refinement was carried out with PEG8000 (14–24% w/v). To further improve crystal quality, micro-seeding was also applied as described before [17] in reservoir solution with 20% and 18% PEG8000. After 3 days, better separated and slightly larger single crystals were obtained (Fig. 3D). Further crystallization refinement, characterization and confirmation of these putative IRAP-inhibitor complex crystals are needed in order to obtain high diffraction quality crystals for future structure determination.

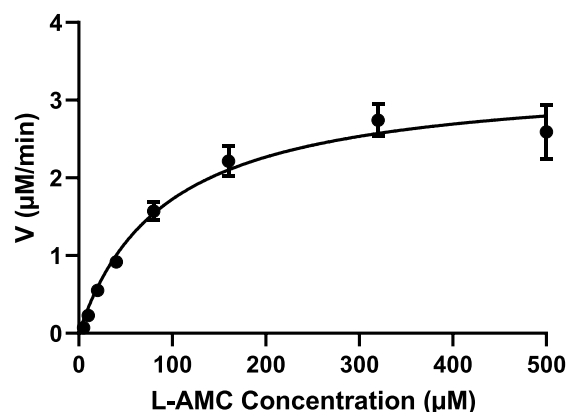
3.4. K_m determination of L-AMC by fluorescence assay

To characterize the enzymatic activity of the purified recombinant IRAP, we measured its catalysis with a commonly used aminopeptidase substrate L-AMC [21]. Hydrolysis activity was measured at different concentrations of the fluorescent substrate L-AMC, as shown in Fig. 4A. V_{max} , K_m , and k_{cat} for L-AMC were calculated by the Michaelis-Menten modeling to be $3.31 \pm 0.15 \mu\text{M}/\text{min}$, $92.0 \pm 12.2 \mu\text{M}$, and $15.7 \pm 0.7 \text{ s}^{-1}$, respectively. This K_m estimate is close to the value ($47.1 \pm 6.2 \mu\text{M}$) reported in the literature [28].

3.5. K_i determination of peptide inhibitor

As an interesting feature of IRAP function, inhibiting IRAP activity has been shown to be a plausible way of enhancing memory [13,14]. To characterize inhibition of the purified IRAP, we select a short peptide inhibitor (VYPWT). Since this pentapeptide is shorter than Ang IV yet still be a potent inhibitor [11], it could provide mechanistic insights as a minimalist strategy for targeted inhibition. To this end, inhibition constant IC_{50} and K_i of this peptide on IRAP catalysis with $80 \mu\text{M}$ substrate L-AMC was determined by plotting the enzymatic activity (percentage) against various peptide inhibitor concentrations (in logarithm), as shown in Fig. 4B. Appears that up to $10 \mu\text{M}$ the peptide still did not achieve a full inhibition, probably due to peptide's turnover after an extended incubation during the assays. Based on this titration, the inhibition constant IC_{50} was calculated to be 184 nM . In the case of competitive inhibition such as in this study, K_i constant can be calculated from IC_{50} with the known substrate concentration, based on the Cheng Prusoff relationship [22]: $IC_{50} = K_i (1 + [S]/K_m)$. Using the K_m

A.



B.

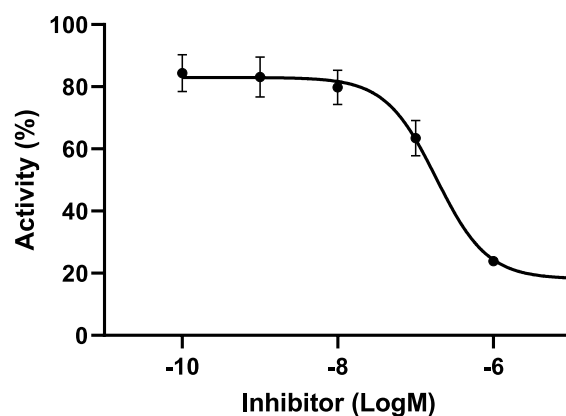


Fig. 4. Kinetic analyses of the recombinant IRAP. A. Purified IRAP was used to determine the catalytic parameters using L-AMC as a substrate. Initial rates (V) were calculated based on duplicates. B. Titration curve of the peptide inhibitor (VYPWT). IRAP activity was quantified using L-AMC in the presence of increasing concentrations of the inhibitor, in log concentrations. Percentage activity was calculated based on activity of control representing full reaction without the peptide inhibitor. Error bars represent standard errors of three replicates.

determined above ($92 \mu\text{M}$), K_i was therefore calculated to be about 98 nM , which is similar to the K_i value reported in the literature— 113 nM [12].

4. Conclusions

IRAP functions in different locations and pathways from ERAP1 and ERAP2 for MHC-I antigen presentation [4,6]. In addition to its immunological importance, IRAP is also a potential memory enhancing target for cognition improvement [13,14]. For most of the IRAP characterization studies reported so far, the recombinant protein was expressed with relatively low yields using mammalian cells such as HEK or COS7 cells, or insect cells sf9 or sf21 [8,9,15,16,26,28]. To facilitate biochemical, biophysical and structural studies of this important enzyme, we describe in this report a yield-increased strategy by expressing recombinant IRAP using High Five insect cell secreted protein expression system to avoid misfolding and insolubility issues. Also comparing to mammalian cell culture, insect cell culture is typically more cost-effective, easier to operate and maintain in suspension. After optimizing protein expression and purification steps, we report here an

increased yield of recombinant IRAP (2–3 mg protein produced from 5-L insect cell culture). This yield appears to be significantly higher than previously reported systems, and with crystallographic purity and high enzyme specific activity. For example by comparing to a previous system with a yield of 1–2 mg/10-L [9], yield in this report has a 3–4 fold increase, likely due to unique features in current protocols such as using HBM secretion signal, High Five insect cells, and additional IEX and/or SEC purification steps. Biochemical characterizations indicate the purified IRAP is functional with a K_m and K_i comparable to those published on literature. In addition, promising IRAP crystals in the presence a potent short peptide inhibitor (VYPWT) have been obtained in the initial crystallization screens. Although confirmation studies still needed for these putative complex crystals, they provide promising conditions for further refinement to obtain diffraction-quality crystals required for future high-throughput and high-resolution crystallographic studies to investigate various IRAP/ligand interactions. Such structural studies in a systematic manner are essential in providing a fundamental understanding in IRAP catalysis and inhibition mechanisms. It will also generate new insights on IRAP substrate specificities to lay a foundation for a rational design of high affinity inhibitors as potential therapeutics in treating memory loss.

Declaration of competing interest

None.

Acknowledgements

We thank Dr. Suchita Pande for helpful discussions, Leah Gens, Reyna Chang, Brendan Lucas and Adam Luk on manuscript preparation. This work was supported by Grant GM128152 from the National Institutes of Health.

References

- [1] D. Descamps, I. Evnouchidou, V. Caillens, C. Drajac, S. Riffault, P. van Endert, L. Saveanu, The role of insulin regulated aminopeptidase in endocytic trafficking and receptor signaling in immune cells, *Frontiers in Molecular Biosciences* 7 (2020) 583556.
- [2] N. Ito, S. Nomura, A. Iwase, T. Ito, F. Kikkawa, M. Tsujimoto, S. Ishiura, S. Mizutani, ADAMs, a disintegrin and metalloproteinases, mediate shedding of oxytocinase, *Biochem. Biophys. Res. Commun.* 314 (2004) 1008–1013.
- [3] M. Tsujimoto, A. Hattori, The oxytocinase subfamily of M1 aminopeptidases, *Biochim. Biophys. Acta* 1751 (2005) 9–18.
- [4] A.L. Hanson, C.J. Morton, M.W. Parker, D. Bessette, T.J. Kenna, The genetics, structure and function of the M1 aminopeptidase oxytocinase subfamily and their therapeutic potential in immune-mediated disease, *Hum. Immunol.* 80 (2019) 281–289.
- [5] D. Fruci, P. Romania, V. D'Alicandro, F. Locatelli, Endoplasmic reticulum aminopeptidase 1 function and its pathogenic role in regulating innate and adaptive immunity in cancer and major histocompatibility complex class I-associated autoimmune diseases, *Tissue Antigens* 84 (2014) 177–186.
- [6] L. Saveanu, J. Babbior, M. Lawand, P. van Endert, Insulin-regulated aminopeptidase and its compartment in dendritic cells, *Mol. Immunol.* 55 (2013) 153–155.
- [7] L.D. Rogers, L.J. Foster, The dynamic phagosomal proteome and the contribution of the endoplasmic reticulum, *Proc. Natl. Acad. Sci. U. S. A.* 104 (2007) 18520–18525.
- [8] H. Matsumoto, T. Rogi, K. Yamashiro, S. Kodama, N. Tsuruoka, A. Hattori, K. Takio, S. Mizutani, M. Tsujimoto, Characterization of a recombinant soluble form of human placental leucine aminopeptidase/oxytocinase expressed in Chinese hamster ovary cells, *Eur. J. Biochem.* 267 (2000) 46–52.
- [9] S.J. Hermans, D.B. Ascher, N.C. Hancock, J.K. Holien, B.J. Michell, S.Y. Chai, C. J. Morton, M.W. Parker, Crystal structure of human insulin-regulated aminopeptidase with specificity for cyclic peptides, *Protein Sci.* 24 (2015) 190–199.
- [10] A.L. Albiston, R.N. Fernando, H.R. Yeatman, P. Burns, L. Ng, D. Daswani, S. Diwakarla, V. Pham, S.Y. Chai, Gene knockout of insulin-regulated aminopeptidase: loss of the specific binding site for angiotensin IV and age-related deficit in spatial memory, *Neurobiol. Learn. Mem.* 93 (2010) 19–30.
- [11] J. Lee, T. Mustafa, S.G. McDowall, F.A. Mendelsohn, M. Brennan, R.A. Lew, A. L. Albiston, S.Y. Chai, Structure-activity study of LVV-hemorphin-7: angiotensin AT4 receptor ligand and inhibitor of insulin-regulated aminopeptidase, *J. Pharmacol. Exp. Therapeut.* 305 (2003) 205–211.
- [12] R.A. Lew, T. Mustafa, S. Ye, S.G. McDowall, S.Y. Chai, A.L. Albiston, Angiotensin AT4 ligands are potent, competitive inhibitors of insulin regulated aminopeptidase (IRAP), *J. Neurochem.* 86 (2003) 344–350.
- [13] N. Barlow, P.E. Thompson, IRAP inhibitors: M1-aminopeptidase family inspiration, *Front. Pharmacol.* 11 (2020) 585930.
- [14] D. Georgiadis, A. Ziotopoulou, E. Kaloumenou, A. Lelis, A. Papisava, The discovery of insulin-regulated aminopeptidase (IRAP) inhibitors: a literature review, *Front. Pharmacol.* 11 (2020) 585838.
- [15] A. Mpakali, E. Saridakis, K. Harlos, Y. Zhao, A. Papakyriakou, P. Kokkala, D. Georgiadis, E. Stratikos, Crystal structure of insulin-regulated aminopeptidase with bound substrate analogue provides insight on antigenic epitope precursor recognition and processing, *J. Immunol.* 195 (2015) 2842–2851.
- [16] A. Mpakali, E. Saridakis, K. Harlos, Y. Zhao, P. Kokkala, D. Georgiadis, P. Giastas, A. Papakyriakou, E. Stratikos, Ligand-induced conformational change of insulin-regulated aminopeptidase: insights on catalytic mechanism and active site plasticity, *J. Med. Chem.* 60 (2017) 2963–2972.
- [17] L. Sui, A. Gandhi, H.-C. Guo, Single-chain expression and crystallization of an antigenic C-terminus in complex with the regulatory domain of ER aminopeptidase 1, *Cryst. Struct. Theor. Appl.* 4 (2015) 47–52.
- [18] L. Sui, A. Gandhi, H.-C. Guo, Crystal structure of a polypeptide's C-terminus in complex with the regulatory domain of ER aminopeptidase 1, *Mol. Immunol.* 80 (2016) 41–49.
- [19] Y.B. Wang, Z.Y. Wang, H.Y. Chen, B.A. Cui, Y.B. Wang, H.Y. Zhang, R. Wang, Secretory expression of porcine interferon-gamma in baculovirus using HBM signal peptide and its inhibition activity on the replication of porcine reproductive and respiratory syndrome virus, *Vet. Immunol. Immunopathol.* 132 (2009) 314–317.
- [20] T.J. Wickham, G.R. Nemerow, Optimization of growth methods and recombinant protein production in BTI-Tn-5B1-4 insect cells using the baculovirus expression system, *Biotechnol. Prog.* 9 (1993) 25–30.
- [21] Y. Kanaoka, T. Takahashi, H. Nakayama, A new fluorogenic substrate for aminopeptidase, *Chem. Pharm. Bull. (Tokyo)* 25 (1977) 362–363.
- [22] Y. Cheng, W.H. Prusoff, Relationship between the inhibition constant (K_i) and the concentration of inhibitor which causes 50 per cent inhibition (I_{50}) of an enzymatic reaction, *Biochem. Pharmacol.* 22 (1973) 3099–3108.
- [23] A. Gandhi, D. Lakshminarasimhan, Y. Sun, H.-C. Guo, Structural insights into the molecular ruler mechanism of the endoplasmic reticulum aminopeptidase ERAP1, *Sci. Rep.* 1 (2011) 186.
- [24] R. Gupta, S. Brunak, Prediction of glycosylation across the human proteome and the correlation to protein function, *Pac. Symp. Biocomput.* (2002) 310–322.
- [25] S.P. Ferris, V.K. Kodali, R.J. Kaufman, Glycoprotein folding and quality-control mechanisms in protein-folding diseases, *Disease Models & Mech.* 7 (2014) 331–341.
- [26] D.B. Ascher, B.A. Cromer, C.J. Morton, I. Volitakis, R.A. Cherny, A.L. Albiston, S. Y. Chai, M.W. Parker, Regulation of insulin-regulated membrane aminopeptidase activity by its C-terminal domain, *Biochemistry* 50 (2011) 2611–2622.
- [27] A. Mpakali, E. Saridakis, P. Giastas, Z. Maben, L.J. Stern, M. Larhed, M. Hallberg, E. Stratikos, Structural basis of inhibition of insulin-regulated aminopeptidase by a macrocyclic peptidic inhibitor, *ACS Med. Chem. Lett.* 11 (2020) 1429–1434.
- [28] A.L. Albiston, V. Pham, S. Ye, L. Ng, R.A. Lew, P.E. Thompson, J.K. Holien, C. J. Morton, M.W. Parker, S.Y. Chai, Phenylalanine-544 plays a key role in substrate and inhibitor binding by providing a hydrophobic packing point at the active site of insulin-regulated aminopeptidase, *Mol. Pharmacol.* 78 (2010) 600–607.